Heteroepitaxial graphite on $6H$-SiC(0001): Interface formation through conduction-band electronic structure

I. Forbeaux, J.-M. Themlin,* and J.-M. Debever

*Groupe de Physique des Etats Condensés, UMR CNRS 6631, Case 901, Faculté des Sciences de Luminy,
F-13288 Marseille Cedex 9, France*

When annealed at elevated temperatures under vacuum, silicon carbide surfaces show a tendency towards graphitization. Using the sensitivity of empty conduction-band states dispersion towards the structural quality of the overlayer, we have used angular-resolved inverse photoemission spectroscopy (KRIPES) to monitor the progressive formation of crystalline graphite on $6H$-SiC(0001) surfaces. The KRIPES spectra obtained after annealing at 1400 °C are characteristic of azimuthally oriented, graphite multilayers of very good single-crystalline quality. For lower annealing temperatures, the ordered interface already presents most of the fingerprints of graphite as soon as 1080 °C. The observation of unshifted π^* states, which reveals a very weak interaction with the substrate, is consistent with the growth of a van der Waals heteroepitaxial graphite lattice on top of silicon carbide, with a coincidence lattice of $(6\sqrt{3}\times 6\sqrt{3})R30°$ symmetry. The growth of the first graphene sheet proceeds on top of adatoms characteristic of the $(\sqrt{3}\times\sqrt{3})R30°$ reconstruction. These adatoms reduce the chemical reactivity of the substrate. A strong feature located at 6.5 eV above the Fermi level is attributed to states derived from Si vacancies in the C-rich subsurface layers of the SiC substrate. This strongly perturbed substrate can be viewed as a diamondlike phase which acts as a precursor to graphite formation by collapse of several layers. In this framework, previously published soft x-ray photoemission spectra find a natural explanation. [S0163-1829(98)06347-4]

I. INTRODUCTION

There has recently been a renewal of interest in graphite,[1] the archetype layered material, in connection with the progress on new allotropic forms of carbon such as nanoclusters (buckyballs) or nanotubes.[2,3] Graphite is made of honeycomb carbon layers weakly coupled to their neighbors. From the theoretical side, much of its unique properties such as Fermi-surface shape or free-carrier density have been tackled by *ab initio* calculations.[4,5] However, apart from some studies which report the use of natural or synthetic single crystals,[6–8] most of the experimental studies to date still rely on the highly oriented pyrolytic graphite (HOPG) material. HOPG, made of an aggregate of small crystallites with random in-plane orientation and separated by regions with translational and rotational disorder, only mimics the perfect arrangement found in true single crystals. In some cases, defects of HOPG-like stacking-fault planes largely determines the measured physical quantity.[1] In the present work, we demonstrate that millimeter-sized bulklike single-crystalline graphite can easily be formed by thermal annealing under vacuum as epitaxial thin films on a silicon carbide wafer. Using surface-sensitive techniques, we reveal some of the mechanisms that govern the formation of the heteroepitaxial graphite layers.

With outstanding characteristics such as wide band gap, high electron saturation velocity, and high thermal, mechanical and chemical stability, silicon carbide presents a great potential for applications in high-temperature, high-frequency, and high-power semiconductor devices. Various polytypes of this material are now commercially available, but to date most of the studies have been carried out on the hexagonal $6H$ and on the cubic polytype $3C$. Their polar surfaces with a silicon termination, $6H$-SiC(0001) and $3C$-SiC(111), present the same stacking sequence down to four Si-C bilayers from the surface.[9] Low-energy-electron-diffraction (LEED) (Refs. 9–11) has revealed several surface reconstructions which have also been studied using techniques such as Auger-electron spectroscopy (AES),[9,12,13] electron-energy-loss spectroscopy (EELS),[12–14] x-ray photoemission spectroscopy (XPS),[12] ultraviolet photoemission spectroscopy (UPS),[15,16] and scanning tunneling microscopy (STM).[17–21] In the present work, we are concerned with the silicon termination of $6H$-SiC which presents several ordered reconstructions with a remarkable range of stoichiometries. Annealing around 850 °C under a Si flux gives a silicon-rich (3×3) reconstruction. A further annealing around 1050 °C gives a $(\sqrt{3}\times\sqrt{3})R30°$ reconstruction made of Si adatoms in the hollow sites of a compact Si termination.[20,22,23] After annealing at 1400 °C, electron diffraction reveals a graphitic termination with only the 1×1 spots of crystalline graphite.[24]

The intermediate step towards graphitization is the $(6\sqrt{3}\times 6\sqrt{3})R30°$ reconstruction (hereafter referred to as $6\sqrt{3}$ for short) obtained after annealing at intermediate temperatures above 1050 °C and below 1300 °C. In their early LEED observations, Van Bommel *et al.*[24] have observed that successive heat treatments of the $6\sqrt{3}$-reconstructed surface lead to a diffraction pattern where only the graphite spots remain visible. AES studies performed on that reconstruction[9,12,13] have also shown that heat treatments above 1000 °C decrease the intensity of the Si peak (88 eV) while the C peak (271 eV) progressively changes from the ''carbide'' type to the ''graphite'' type, its intensity remaining constant. The same behavior has also been observed by EELS,[12] where, after annealing at 1000 °C, a sharp loss feature characteristic of

graphite appears in the electron energy loss spectrum. From a vibrational point of view, optical phonons of the graphite layer have been detected by HREELS.[14] The structure of the 6*H*-SiC(0001) termination has also been probed by atom-resolved microscopies. STM has revealed[17–19] that annealing the surface at 1150 °C induces the formation of a 6×6 reconstruction corresponding to the $(6\sqrt{3}\times6\sqrt{3})R30°$ pattern observed in previous LEED studies.

All these studies roughly converge towards the same conclusion: the $(6\sqrt{3}\times6\sqrt{3})R30°$ reconstruction consists of an independent graphite layer on top of the unreconstructed surface of 6*H*-SiC(0001). However, a recent high-resolution core-level photoemission study of the $(6\sqrt{3}\times6\sqrt{3})$ $R30°$-reconstructed surface cast some doubt on this picture.[15] On the one hand, these authors have demonstrated that the $(6\sqrt{3}\times6\sqrt{3})R30°$ reconstruction contains a considerably larger amount of carbon than silicon compared to the $(\sqrt{3}\times\sqrt{3})R30°$ structure. They have concluded that the structural changes from the $\sqrt{3}$ to the $6\sqrt{3}$ are accompanied by changes in the chemical composition of the surface along the trends given by the above-mentioned AES studies.[9,12,13] On the other hand, they have followed the evolution of high-resolution C 1*s* and Si 2*p* UPS spectra after heating at temperatures between 950 and 1350 °C. This leads to surface-shifted C 1*s* components with binding energies *different from the graphitic C 1s peak*, since both bulk and surface-sensitive spectra are characterized by features at higher binding energies. For the $\sqrt{3}$ surface, the C 1*s* surface-sensitive spectra are dominated by one broad feature around 283.5 eV and another broad, weak feature located around 285 eV. The intensity of this last feature dominates the spectra for annealing temperatures between 1150 and 1250 °C, where the surface exhibits a fully developed $(6\sqrt{3}\times6\sqrt{3})R30°$ LEED pattern. This broad feature can be decomposed into at least two components located at ≈285.5 and 284.7 eV. While the latter is clearly assigned to graphitic carbon, the origin of the former, completely dominant below 1350 °C, is still unclear. Its presence allows Johansson *et al.* to rule out the formation of graphite below 1350 °C. It is only after annealing at 1350 °C that the intensity of the component at 285.5 eV decreases and that the shape of the C 1*s* spectrum becomes that of graphite with practically a single component at 284.7 eV related to sp^2-hybridized graphitic carbon.

As far as the electronic structure of the $6\sqrt{3}$ reconstruction is concerned, it thus seems to significantly differ from the well-known spectroscopic signature of graphite, at least from the core-level shift analysis. Fortunately, this kind of system (Monolayer of graphite/substrate) has long been of great interest in relation to catalysis.[25–27] In some cases, a strong interaction with the substrate has been reported where the overlayer acquires modified structural, vibrational, and electronic properties which can significantly differ from a ''bulk'' graphite layer.[27–29] However, the observation of an ordered superstructure does not favor the idea of a strong overlayer/substrate interaction which is expected to degrade the long-range order within a single layer. New and complementary measurements were thus required to understand the evolution of this complex interface towards the ''graphitized'' termination of 6*H*-SiC(0001). $k_{\parallel}$-resolved inverse-photoemission spectroscopy (KRIPES), involving optical transitions between empty crystal states, is ideally suited to

the study of the electronic structure of layered materials such as graphite.[6] Indeed, highly localized two-dimensional unoccupied states usually generate a significant photon flux upon electron bombardment. Furthermore, from the conservation of the parallel component of the wave vector **k**, we can usually determine a two-dimensional experimental band structure $E(k_{\parallel})$ which can be compared with the calculated, projected empty band structure of the layered solid. Applying KRIPES on 6*H*-SiC(0001), we are able to identify empty π^* states which are clear fingerprints of graphitic carbon for annealing temperatures as low as 1080 °C.

II. EXPERIMENT

The experiments have been performed in an ultrahigh-vacuum chamber (base pressure 10^{-10} mbar) equipped with a low-energy electron diffractometer and the inverse photo-emission system.[30] This one consists of a BaO electron gun and an elliptical mirror to focus photons emitted in a large solid angle toward the photon counter. The Geiger-Müller type detector filled with a helium-iodine mixture and sealed with a CaF_2 window operates in an isochromat mode at a fixed photon energy of 9.7 eV. The overall energy resolution, determined by measuring the Fermi edge of a polycrystalline Ta foil, is 0.6 eV, including the performance of the electron gun and the detector. The angular resolution defined by the dispersion of the electron beam is about 3° resulting in a $\Delta k_{\parallel}<0.1$ Å^{-1}. The dispersion within the surface Brillouin zone (SBZ) of interest is investigated by rotating the electron gun in a vertical plane perpendicular to the sample surface (variable polar angle θ with respect to the surface normal) and oriented along a given azimuth.

We have used a commercial (Cree research), nitrogen-doped ($N_D=9\times10^{17}$ cm^{-3}) 6*H*-SiC(0001) sample cut from a 0.3-mm-thick wafer. The sample was fixed by Mo clips and all the treatments were achieved in a preparation chamber (base pressure $<3\times10^{-10}$ mbar). The temperature of annealing was monitored by an infrared pyrometer assuming an emissivity of 0.90.[13] The 6*H*-SiC(0001) sample is introduced into vacuum without *ex situ* cleaning. The subsequent cleaning steps will be described below (see Sec. III).

III. EXPERIMENTAL RESULTS

A. Overview

Figure 1 shows the KRIPES spectra taken at normal incidence ($\theta=0°$) for different reconstructions of the 6*H*-SiC(0001) surface obtained for increasing values of annealing temperature. The intensities of each spectrum have been normalized to the transmitted sample current. The energies are referenced to the Fermi level measured on a nearby metal in electrical contact with the sample. Figure 2 presents selected LEED patterns observed on these surfaces. Right after introduction into vacuum followed by a moderate annealing below 900 °C, a faint 1×1 pattern (not shown in Fig. 2) related to adsorbed residual O or other contaminants is observed.[11] The corresponding KRIPES spectrum visible in Fig. 1 gives some faint structures. The sample, held at a fixed temperature around 900 °C, is then exposed to a Si flux obtained from a resistively heated Si wafer held near 1200 °C. This cleaning procedure is used to remove the na-
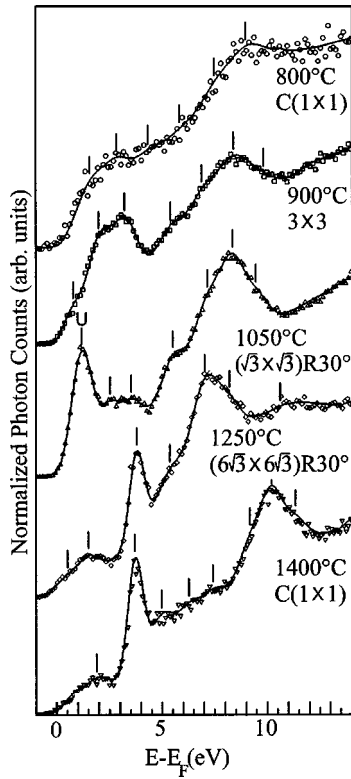
FIG. 1. KRIPES spectra taken at normal incidence ($\theta = 0°$) for different reconstructions of the $6H$-SiC(0001) surface obtained for increasing values of annealing temperature.

tive surface oxides which sublime at this temperature as SiO species.[9] The LEED pattern then exhibits a sharp 3×3 reconstruction [Fig. 2(a)], attributed to a silicon-rich termination.[17] A further annealing in the range 1000–1050 °C for a few minutes produces a $(\sqrt{3} \times \sqrt{3})R30°$ reconstruction [Fig. 2(b)], attributed to Si adatoms occupying the filled T_4 sites above a compact bilayer termination.[20,22] In inverse photoemission, this reconstruction is characterized by a sharp peak U (Fig. 1) appearing 1.1 eV above the Fermi level and attributed to an empty surface state.[23] Other structures with a maximum around 7.5 eV above the Fermi level are much less sensitive to contamination and can be ascribed to bulk states. Successive heat treatments at higher temperatures (above 1080 °C) induce the gradual development of a complex $(6\sqrt{3} \times 6\sqrt{3})R30°$ pattern [Figs. 2(c)–2(e)]. This pattern has been interpreted considering a crystalline single graphite monolayer on top of SiC, rotated by 30° with respect to the SiC lattice.[24] At low annealing temperatures, the SiC spots are the brightest. Figure 3(a) shows a LEED pattern ($E_P = 110$ eV) taken after annealing around 1100 °C. Figure 3(b) shows the unit vectors s_1 and s_2 of the SiC reciprocal lattice. c_1 and c_2, the unit vectors of the reciprocal lattice of the overlayer, are determined from the LEED pattern obtained after annealing at 1400 °C [Fig. 2(f)]. Taking as a reference the substrate lattice constant at 3.07 Å,[31] the lattice constant of the overlayer is estimated at 2.4 ± 0.1 Å from the LEED pattern. This value can be compared with the reported[4] value for graphite, $a = 2.4589$ Å. The diffraction pattern is thus consistent with a graphite overlayer with its
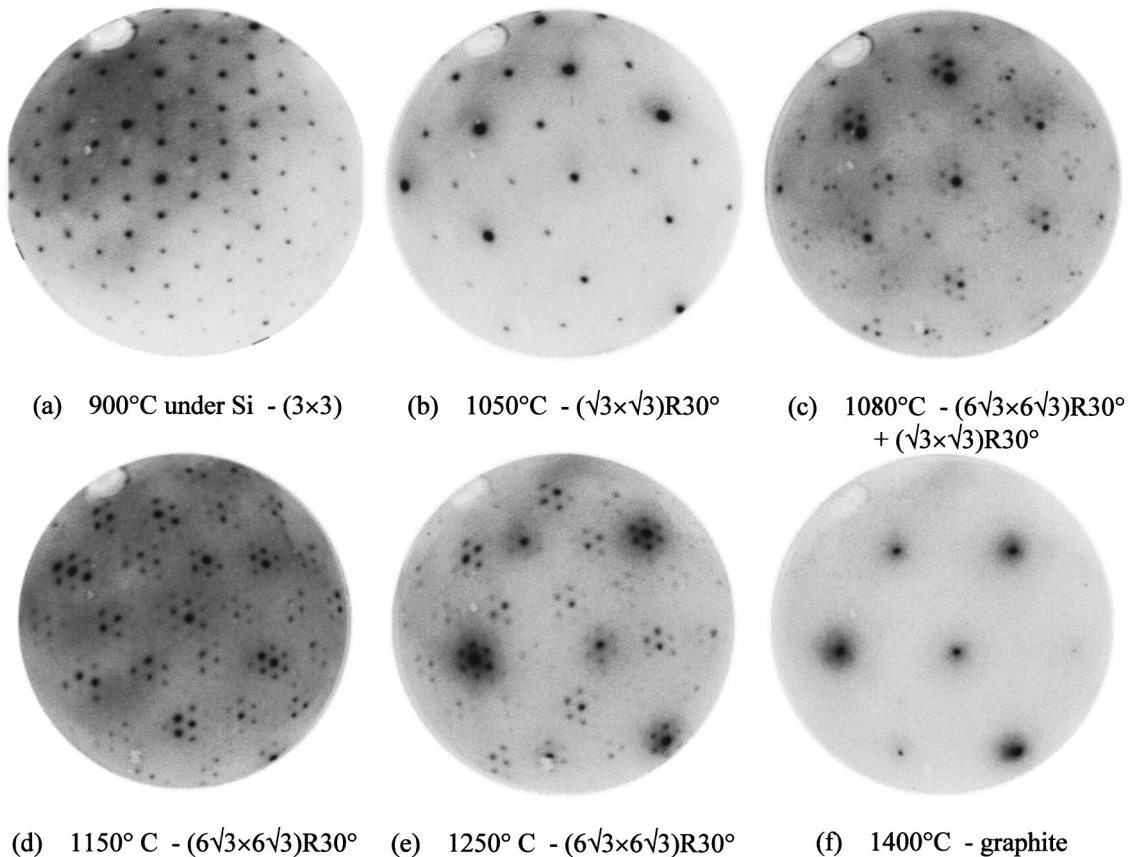

(a)   900°C under Si - (3×3)   (b)   1050°C - (√3×√3)R30°   (c)   1080°C - (6√3×6√3)R30°
                                                                    + (√3×√3)R30°

(d)   1150° C - (6√3×6√3)R30°   (e)   1250° C - (6√3×6√3)R30°   (f)   1400°C - graphite

FIG. 2. LEED patterns from $6H$-SiC(0001) with a primary energy of 130 eV obtained on (a) (1×1), (b) $(\sqrt{3} \times \sqrt{3})R30°$, (c) $(\sqrt{3} \times \sqrt{3})R30°$ and $(6\sqrt{3} \times 6\sqrt{3})R30°$, (d) and (e) $(6\sqrt{3} \times 6\sqrt{3})R30°$, and (f) graphite (1×1).
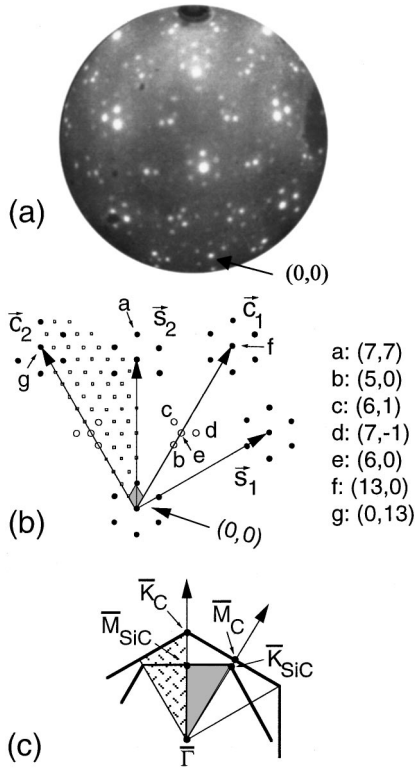
FIG. 3. (a) LEED pattern of 6H-SiC(0001) with a primary energy of 110 eV after Si flux exposure (see text) and annealing around 1100 °C. (b) Schematics of the diffracted beams, showing the unit vectors s_1 and s_2 of the SiC reciprocal lattice and c_1 and c_2, the unit vectors of the reciprocal lattice of the overlayer. Other spots are visible which are located at the positions of sum vectors of substrate and overlayer reciprocal-lattice vectors. The position of these spots is given by the reciprocal vector $n\mathbf{r}_1 + m\mathbf{r}_2$ and labeled by (n,m), where $\mathbf{r}_1$ and $\mathbf{r}_2$ are the basis vectors of the small $(6\sqrt{3} \times 6\sqrt{3})R30°$ unit mesh (shaded) in the reciprocal space. (c) In the reciprocal space, because of the 30° rotation between the substrate and the overlayer, the $\overline{\Gamma}$-$\overline{K}$ direction of the graphite SBZ corresponds to the $\overline{\Gamma}$-$\overline{M}$ direction of the SiC SBZ and *vice versa*.

$\langle 21\overline{3}0 \rangle$ azimuth oriented along the substrate $\langle 11\overline{2}0 \rangle$ azimuth. For that orientation, a coincidence lattice with a large hexagonal unit cell of a $(6\sqrt{3} \times 6\sqrt{3})R30°$ symmetry[19] with respect to the substrate is obtained. In the reciprocal space, because of the 30° rotation between the substrate and the overlayer, the $\overline{\Gamma}$-$\overline{K}$ direction of the graphite SBZ corresponds to the $\overline{\Gamma}$-$\overline{M}$ direction of the SiC SBZ and *vice versa* [Fig. 3(c)]. Other spots are visible which are located at the positions of sum vectors of substrate and overlayer reciprocal-lattice vectors. The position of these spots is given by the reciprocal vector $n\mathbf{r}_1 + m\mathbf{r}_2$ and labeled by (n,m), where $\mathbf{r}_1$ and $\mathbf{r}_2$ are the basis vectors of the small $(6\sqrt{3} \times 6\sqrt{3})R30°$ unit mesh in the reciprocal space. For example, spot (7,7) in Figs. 3(a) and 3(b) is obtained by adding one overlayer reciprocal vector $\mathbf{c}_1 + \mathbf{c}_2$ to one substrate vector $-\mathbf{s}_2$. Similarly, spot (5,0) is given by $(\mathbf{s}_1 + \mathbf{s}_2) - \mathbf{c}_1$, spot (6,1) by $\mathbf{c}_2 + (\mathbf{s}_1 - \mathbf{s}_2)$, and spot (7,−1) by $(\mathbf{c}_1 - \mathbf{c}_2) + (\mathbf{s}_2 - \mathbf{s}_1)$. Other spots of the $(6\sqrt{3} \times 6\sqrt{3})R30°$ mesh may be obtained by combination of other reciprocal vectors. However, most of these combinations involve large reciprocal-lattice vectors that will produce a much lower intensity in the

double diffraction process involved.[32] Indeed, some of these spots are visible, although faint, on the LEED pattern photograph of Fig. 3(a), obtained after annealing around 1100 °C. In particular, this should also be the case for the (6,0) spot which is also part of the smaller adatom-induced $(\sqrt{3} \times \sqrt{3})R30°$ reconstruction of the substrate. However, this spot remains perfectly visible up to about 1100 °C. This shows that besides multiple diffraction, single diffraction by the $(\sqrt{3} \times \sqrt{3})R30°$ reconstruction which coexists with the $6\sqrt{3}$ reconstruction[33] on different terraces most probably contributes to the (6,0) spot intensity. Although this spot is part of the $(6\sqrt{3} \times 6\sqrt{3})R30°$ pattern, its intensity suddenly decreases above 1100 °C where it becomes indistinguishable from the background. This is consistent with the disappearance, at this temperature, of the unoccupied surface-state peak in the inverse-photoemission spectrum since both the empty surface state and the (6,0) spots are directly related to the presence of adatoms. Above the annealing temperature of 1150 °C, the (13,0) and (0,13) spots become more and more intense up to 1400 °C where other multiple-diffraction spots have disappeared [Fig. 2(f)]. These (13,0) and (0,13) spots are coincident with the graphite (1,0) and (0,1) diffracted beams [Fig. 3(b)]. It seems plausible that upon annealing, the overlayer thickness becomes larger than the electron mean free path and the primary electrons can no longer reach the substrate. The growth of given structures in the KRIPES spectra (see below) will prove the gradual development of more than one single layer of graphite. Since the graphite unit cell contains two atoms, the structure factor modulates the diffracted beam intensities by doubling the (h,k) spot intensity where $h+k = \pm 3n$, with $n=0,1,2,...$. The observation of narrow spots instead of the ringlike structures usually observed on HOPG ascertains the good azimuthal ordering of the graphite thin layer. We also note that a lower contrast is observed on the three LEED pattern photographs of Figs. 2(c)–2(e), where the $6\sqrt{3}$ pattern is present. This higher background intensity with respect to the $\sqrt{3}$ or graphite-(1×1) reconstructions suggests some degree of disorder or amorphization. We will show below that this disorder is linked to the presence of silicon vacancies in a carbon-rich phase precursor of graphite formation.

B. Multilayer graphite

As a starting point, we have studied in detail the surface heated at 1400 °C for which the presence of graphitic carbon is evidenced by its characteristic LEED pattern [Fig. 2(f)]. Various studies performed on similarly prepared surfaces have also concluded that after an extended annealing above 1350 °C, the surface is covered by several layers of graphitic carbon.[13] The SXPS and UPS measurements[15] also find clear evidence of graphitization after extended annealing at this elevated temperature. Figure 4 presents spectra recorded on that surface for the two high-symmetry directions of the graphite SBZ. The peak positions, marked by vertical bars, are determined by adjusting a sum of Gaussian line shapes and a background baseline to the raw data (Fig. 5). For all the spectra, the solid line is the envelope of the synthetic spectra obtained from the addition of the Gaussian peaks and the background, and the experimental data are represented
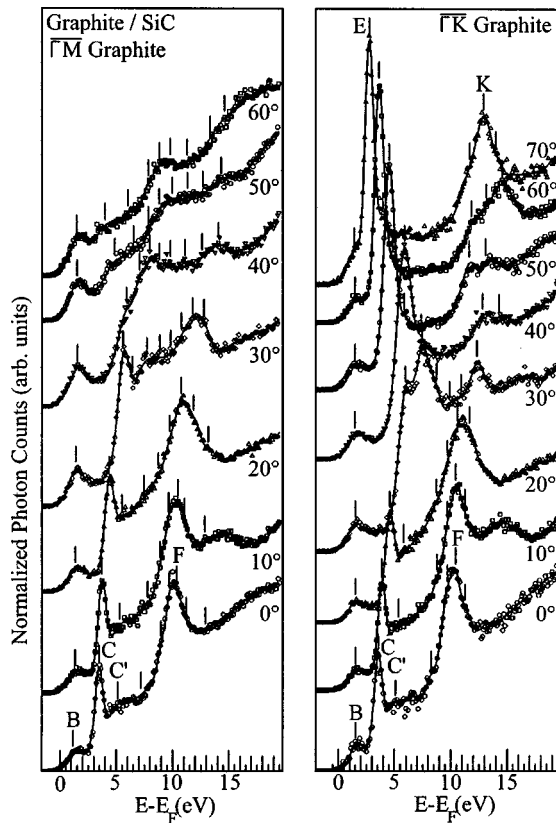
FIG. 4. KRIPES spectra obtained on the graphitized 6H-SiC(0001) surface annealed at 1400 °C as a function of the polar angle θ along the $\bar{\Gamma}$-$\bar{M}$ and $\bar{\Gamma}$-$\bar{K}$ direction of the graphite surface Brillouin zone.

with open circles. For both directions, the spectra are symmetrical with respect to $\theta = 0°$ and present at least five distinct features. We first observe, located at ≈ 1.5 eV above the Fermi level (E_F), a peak B present all over the SBZ with
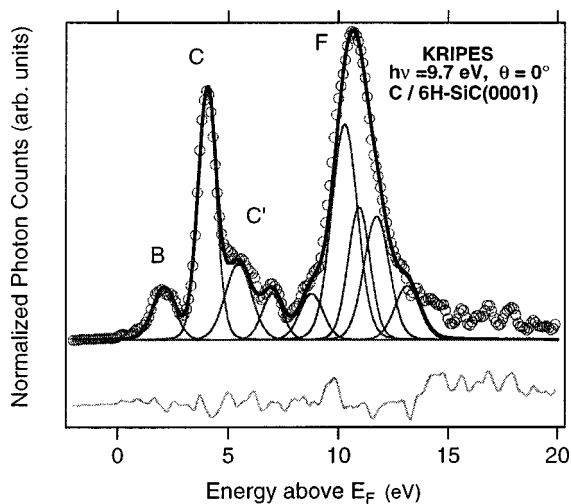

FIG. 5. Example of a set of Gaussians used to fit a KRIPES spectrum obtained at normal incidence on the graphitized 6H-SiC(0001) surface obtained after annealing at 1400 °C. The experimental data (dots) are adjusted with the sum of segments of linear background (substracted from the raw data in this figure) and the fitted set of Gaussians (solid line). The bottom curve shows the residuals between the fit result and the experimental data.
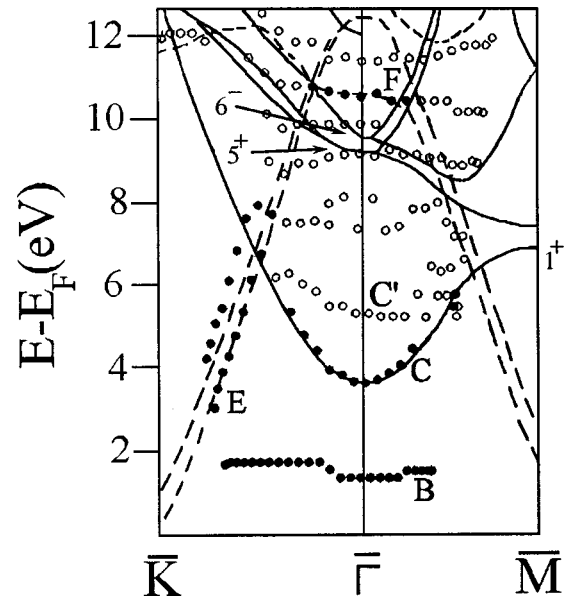

FIG. 6. Final-state energies with respect to E_F versus the wave vector parallel to the surface for the dominant peaks B, C, E, F (filled circles), or shoulders (open circles) of the KRIPES spectra shown in Fig. 4, together with the results of self-consistent band-structure calculations for graphite from Ref. 35. The $\sigma^*(\Gamma_1^+)$ and $\sigma^*(\Gamma_5^+, \Gamma_6^-)$ bands are indexed following the notation used in Ref. 35.

only a slight dispersion. At ≈ 4 eV above E_F at the $\bar{\Gamma}$ point, we note the presence of peak C, very sharp for $|\theta| < 35°$ and disappearing for $|\theta| > 40°$. We can observe the large dispersion of this peak which goes away from E_F by almost 2 eV for increasing values of $|\theta|$. Another very sharp and prominent peak (E) is also present for $|\theta| > 35°$. It can be seen in the $\bar{\Gamma}$-$\bar{K}$ direction of the graphite SBZ and shows a very large dispersion towards E_F for increasing values of $|\theta|$. Spectra also present two other marked features: peak F, located at ≈ 10.5 eV above E_F, observed for $|\theta| < 30°$, and peak K, located at ≈ 13 eV above E_F, appearing for $|\theta| > 55°$ in the $\bar{\Gamma}$-$\bar{K}$ direction of the graphite SBZ.

Graphite has different bonding character depending on the crystallographic orientation. The strong bonding of the C atoms within the basal planes is conveniently described by σ states, contributed to by $2s$ and $2p_{x,y}$ atomic orbitals. The π states made of $2p_z$ orbitals are oriented perpendicular to the planes. Band-structure calculations[34,35] have shown that the low-energy region of the conduction band is of π character, whereas the high-energy part has mainly σ character. The final-state energies with respect to E_F versus the wave vector parallel to the surface are presented in Fig. 6 for the various peaks or shoulders of our KRIPES spectra (Fig. 4), together with the results of self-consistent band-structure calculations for graphite from Holzwarth et al.,[35] abbreviated HLR in what follows. The nondispersing peak B present in all the spectra at ≈ 1.5 eV above E_F has been attributed to indirect transitions into the high density of states of the π^* band at the $\bar{M}$ point.[6] The overall behavior of C located at ≈ 4 eV above E_F in normal incidence and showing an upward dispersion away from $\bar{\Gamma}$ closely follows the calculated dispersion predicted by HLR for the $\sigma^*(\Gamma_1^+)$ state. However, this

nice agreement is fortuitous, since photon-energy-resolved inverse-photoemission experiments[36] have shown that the sharp structure C has no dispersion perpendicular to the basal plane. This is in contrast to the predicted behavior of the $\sigma^*(\Gamma_1^+)$ state. Although graphite is the archetype of a two-dimensional solid, the interaction between layers manifests itself in several ways in the electronic structure such as, e.g., the splitting of the π and π^* bands, calculated by HLR and experimentally observed in ARUPS (Ref. 37) and KRIPES.[6] The interlayer interactions are also responsible for the strong dispersion normal to the basal plane of $\sigma^*(\Gamma_1^+)$, the first unoccupied σ band. Band-structure calculations by HLR reveal that the electron density distribution for this state is highly concentrated in the region between two carbon planes, which is why the $\sigma^*(\Gamma_1^+)$ state is often referred to as the ''interlayer'' state. The $\sigma^*(\Gamma_1^+)$ state has been unambiguously localized[36] as a tiny, strongly dispersing feature located at 5 eV above E_F near $\bar{\Gamma}$. In the present study, the faint structure C' with a parabolic dispersion visible in Fig. 6 can most probably be ascribed to this $\sigma^*(\Gamma_1^+)$ state. Coming back to the sharp structure C, it seems that to date, no consensus has been reached about its origin. Calculations by Posternak *et al.* have predicted an unoccupied surface state located at 3.8 eV above E_F. However, the small sensitivity of peak C to activated O_2^* or H_2^* casts some doubt[38] on its surface origin. Structure C has also been attributed[38,36] to indirect transitions into some high density of states at the bottom of the interlayer state $\sigma^*(\Gamma_1^+)$. Surprisingly, other studies[39] have reported a marked sensitivity of peak C towards contamination. An alternative explanation has therefore been proposed for this prominent peak which could derive from an image-potential surface state. These image-potential states where the incoming electron is trapped by its own Coulombic image force are well known for metal surfaces.[40] On the other hand, by comparing the attenuation of peak C and other bulk-derived structures upon the growth of Au and Pd clusters, Hu *et al.* were able to conclude[41] to the surface-derived origin of the sharp structure C, either a surface state or an image state.

With an asymmetric line shape, peak E is the most prominent structure of our KRIPES spectra. It is observed at high incidence in the $\bar{\Gamma}$-$\bar{K}$ direction, and is readily attributed to the low-lying π^* states which disperse towards the Fermi level reached at the $\bar{K}$ point where it slightly overlaps the filled π bands, since graphite is a semimetal. It should be noted that due to the high incidence angle required, we could not observe the Fermi level crossing at the $\bar{K}$ point at such a low final energy. Spectra have also revealed two other features that can be assigned to known bands of graphite by comparison with KRIPES spectra of earlier studies: a non-dispersive peak F around 10.5 eV that has been readily identified with the antibonding σ^* bands of Γ_5^+,Γ_6^- symmetry at $k=0$, and a pronounced feature **K** occurring for $|\theta|>55°$. In accordance with previous KRIPES results on HOPG (Refs. 39 and 42) or natural graphite single crystal,[6,7] peak K seems to follow the calculated dispersion of the $\pi^*(\Gamma_3^+,K_6)$ band. However, the strong dispersion of this feature towards high energies (visible in the upper two spectra of Fig. 4 at $\theta=60°$ and 70° but not represented in Fig. 6) has no counter-

part in the available high-energy band-structure calculations. Finally, the attribution of peak F to transitions into the antibonding $\sigma^*(\Gamma_5^+,\Gamma_6^-)$ bands near the BZ center deserves some comments since the intensity of peak F will be used below to gain information on the overlayer morphology. Figure 6 shows that the $\sigma^*(\Gamma_5^+,\Gamma_6^-)$ bands strongly disperse in the vicinity of the BZ center. This is in contrast with the limited dispersion experimentally observed on peak F. This can be understood considering that the optical transitions of the electron are supported by a high one-dimensional density of final states normal to the surface. Indeed, according to the band-structure calculations[34,35] the states have no dispersion along the ΓA direction (normal to the surface) of the bulk BZ, resulting in a high DOS at the zone center in the projected band-structure probed by isochromat KRIPES. The observation of peak F thus requires a well-developed band in the $k_\perp$ direction. This is only obtained when a sufficient number of graphitic layers build up and the layered solid acquires a three-dimensional character. We will use below the growth of peak F as a fingerprint for the growth of multilayered graphite.

In conclusion for this part, the spectra recorded on this graphitic surface are of high quality comparable with earlier studies of the conduction-band structure of natural graphite single crystal[6,7] or HOPG.[39,42] Several observed features (peaks C, E, and F) are prominent and very sharp, their widths approaching the resolution of our apparatus. For example, the fit shows that peak E derived from the π^* states can be resolved into two components lying approximately 1 eV apart, in close agreement with the π^* splitting predicted by HLR. Furthermore, marked differences in the spectra between the $\bar{\Gamma}$-$\bar{K}$ and the $\bar{\Gamma}$-$\bar{M}$ directions are found which are evidence of the single crystallinity of these graphitic layers. Hence, we can conclude that at these elevated annealing temperatures above 1350 °C, the substrate is covered by several layers of single-crystalline graphite.

C. The $6\sqrt{3}$ reconstruction

We consider now the surfaces with a well-developed $(6\sqrt{3}\times6\sqrt{3})R30°$ diffraction pattern, obtained for a temperature of annealing of 1150 °C where the $6\sqrt{3}$ reconstruction is uniformly present on the surface. In order to check if some graphitic carbon fingerprints could be identified, we have recorded spectra for various angles along the two high-symmetry directions of the overlayer graphite SBZ (Fig. 7). A structure near 4 eV above E_F immediately reminds peak C of graphite. In the vicinity of the Fermi level, we observe two nondispersive peaks A and B, located at ≈1 and 2 eV above E_F, present all over the SBZ. We observe several other features, such as feature D, located at ≈6.5 eV above E_F, which appears around the $\bar{\Gamma}$ point ($|\theta|<25°$) with a flat dispersion; peak C, located at ≈4 eV above E_F at the $\bar{\Gamma}$ point, very sharp for $|\theta|<35°$ and disappearing for $|\theta|>40°$; and peak E appearing for $|\theta|>35°$ in the $\bar{\Gamma}$-$\bar{M}$ direction of SiC reciprocal space. Because of their energy position and dispersion behavior, the three structures B, C, and E are very close to the case of multilayer graphite. However, the strong peak D near 6.5 eV above E_F and peak A have no equivalent on graphite.
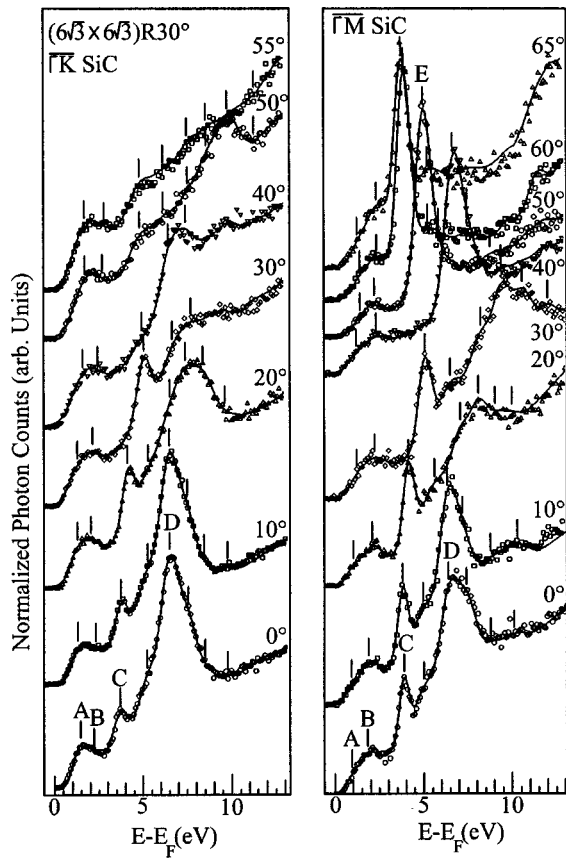
FIG. 7. KRIPES spectra obtained on surfaces with a well-developed $(6\sqrt{3}\times6\sqrt{3})R30°$ diffraction pattern, obtained for a temperature of annealing of 1150 °C. The spectra are obtained for various polar angles along the two high-symmetry directions $\bar{\Gamma}$-$\bar{M}$ and $\bar{\Gamma}$-$\bar{K}$ of the SiC substrate SBZ.
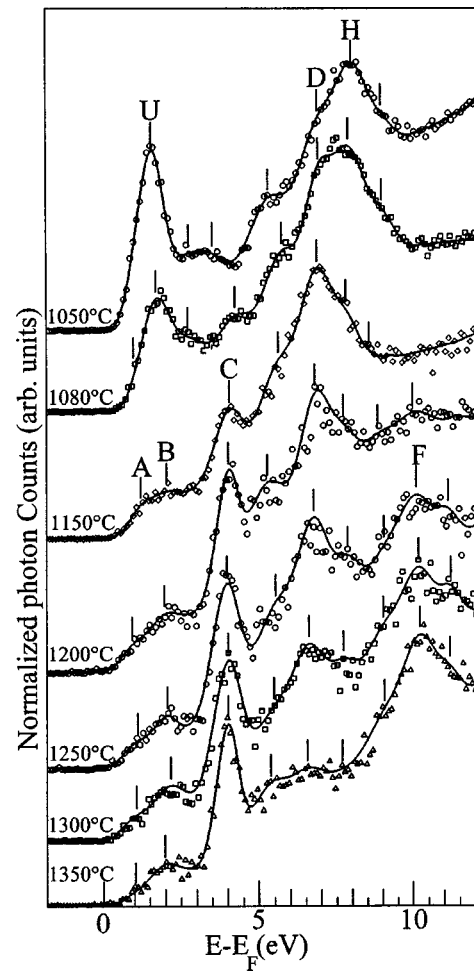

FIG. 8. KRIPES spectra taken at normal incidence ($\theta=0°$) on $6H$-SiC(0001) surfaces annealed for increasing values of annealing temperatures from 1050 °C up to 1350 °C.

To understand the origin of feature D, strong around $\bar{\Gamma}$, we have followed the KRIPES spectra at normal incidence for different annealing temperatures from 1050 °C up to 1400 °C (Fig. 8). A detailed decomposition of all these spectra shows that peak D, dominant in the range of temperature 1100–1200 °C, is already present as a shoulder on the $(\sqrt{3}\times\sqrt{3})R30°$ reconstructed surface. The spectra taken on the $(\sqrt{3}\times\sqrt{3})R30°$ surface present a surface state U (Ref. 23) and a large structure around 8 eV that has been decomposed into three components with D and H at 6.5 and 7.5 eV above E_F (Fig. 9). At 1080 °C, the intensity of the surface state U is reduced and a new feature at ≈4 eV above E_F begins to appear. Because of its energy position and its evolution upon annealing, this peak can be assimilated to peak C on the graphite spectra, suggesting that graphite formation already proceeds at 1080 °C. We can also note that the intensity of D is stronger than for the $\sqrt{3}$ surface while the intensity of H diminishes. In the detailed spectral decomposition of Fig. 9, it is clear that in the range 1050–1150 °C, the growth of D goes on at the expense of H. D becomes the dominant structure in this temperature region where the $6\sqrt{3}$ reconstruction is fully developed. At 1200 °C, we observe the emergence of a new feature at ≈9.5 eV above E_F. This feature corresponds to the previously described peak F because of its energy position and intensity evolution upon heat treatments up to 1350 °C. We have seen earlier that this structure is

associated with the $\sigma^*(\Gamma_5^+,\Gamma_6^-)$ bands of graphite, which reveals the growth of multilayered graphite with a marked 3D character. At higher temperature, above 1300 °C, the intensities of the two structures D and H are reduced and at 1350 °C the spectra are characteristic of graphite with peak C and F very well developed.

To probe the presence of carbon graphite on the surface as early as 1080 °C, we have followed the evolution of spectra taken at a high angle of incidence for which a very characteristic peak of graphite, namely the π^* band, appears very sharp and prominent. Figure 10 presents the spectra recorded at $\theta=55°$ along the $\bar{\Gamma}$-$\bar{K}$ direction of the graphite SBZ for different annealing temperatures corresponding to Fig. 8. We can note the presence of peak E as early as 1080 °C. Its intensity is larger after each annealing while its energy position does not change at all. So, as early as 1080 °C, we can unambiguously observe some fingerprints of graphite with π^* and σ^* bands. The lack of a significant energy shift on the position of the sensitive π^* states with respect to the "bulk" graphite reveals a weak interaction with the substrate. In particular, it rules out a significant charge transfer between the overlayer and the substrate. It also rules out a strong rehybridization of some carbon orbitals with other orbitals of the substrate. Such a rehybridization would show
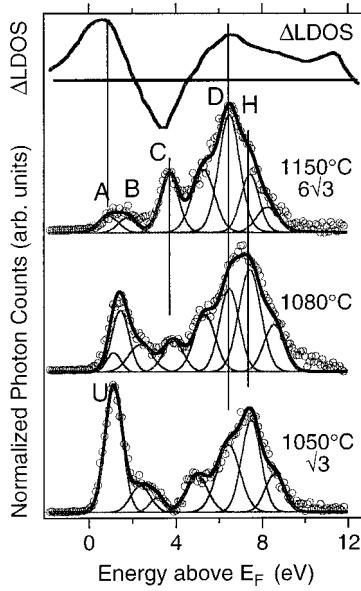
FIG. 9. Decomposition of selected KRIPES spectra for three annealing temperatures of 1050 °C [$(\sqrt{3} \times \sqrt{3})R30°$], 1080 °C [coexistence of $(\sqrt{3} \times \sqrt{3})R30°$ and $(6\sqrt{3} \times 6\sqrt{3})R30°$], and 1150 °C [$(6\sqrt{3} \times 6\sqrt{3})R30°$]. The top curve shows the result of a calculation on bulk defective β-SiC (Ref. 47): it represents the changes in local density of states (Δ-LDOS) around a Si vacancy.

up as a deformation of the π^* bands which are known to be very sensitive to rehybridization.[27]

IV. DISCUSSION

The picture which emerges from the whole set of results is a model where, since the beginning of its formation (above 1080 °C), an ordered graphite overlayer interacts with the SiC substrate through weak van der Waals forces. Long-
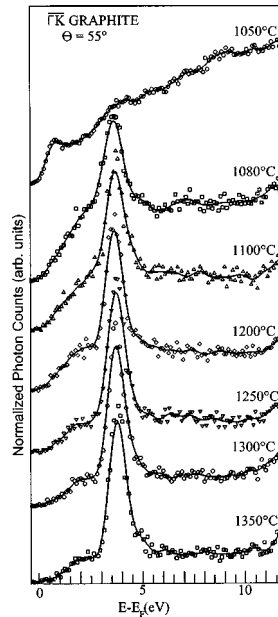

FIG. 10. KRIPES spectra recorded at a polar angle $\theta = 55°$ along the $\bar{\Gamma}$-$\bar{K}$ direction of the graphite SBZ for different annealing temperatures corresponding to Fig. 8. We can note the presence of the peak E as early as 1080 °C.
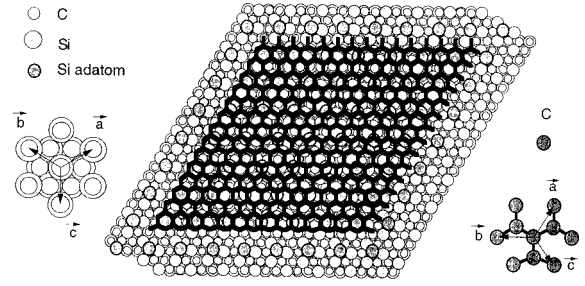

FIG. 11. Ball model representing part of a graphite overlayer on top of a Si-adatom-covered 6H-SiC(0001) substrate (silicon termination). The graphite $\langle 21\bar{3}0 \rangle$ azimuth is oriented along the substrate $\langle 11\bar{2}0 \rangle$ azimuth. For that specific orientation, a coincidence lattice with a large hexagonal unit cell of a $(6\sqrt{3} \times 6\sqrt{3})R30°$ symmetry with respect to the substrate is obtained. The Si adatoms at the four edges of the represented graphene sheet coincide with troughs of the honeycomb graphite and are thus four nodes of the $(6\sqrt{3} \times 6\sqrt{3})R30°$ coincidence lattice. Note that for clarity, the carbon atoms of the graphene sheet are not represented, only bonds between C atoms reveal the graphite honeycomb layer.

range order is obtained through the intralayer interactions which are stronger than the overlayer-substrate interactions. This is similar to the process known as Van der Waals epitaxy, where the formation of sharp and defect-free interfaces between 2D and 3D materials has been reported.[43] In the present case, however, the material for the overlayer formation does not come from the gas phase but rather from the substrate itself. In both cases, the unreactive character of the "substrate" surface is essential to preserve the crystalline character of the overlayer. The LEED results have evidenced the coexistence of both $\sqrt{3}$ and $6\sqrt{3}$ reconstructions in the early stage of $6\sqrt{3}$ formation around 1100 °C. Although some heterogeneity in the termination among different terraces cannot be ruled out,[33] the persistence of the surface state U suggests that the initial $6\sqrt{3}$ formation may proceed on top of an adatom-terminated substrate of $\sqrt{3}$ symmetry, at least in the very beginning of graphite growth. This is a favorable case since the number of dangling bonds which would be present at a compact Si termination is reduced by $\frac{1}{3}$ due to the presence of Si adatoms. Furthermore, the remaining surface states localized on the adatoms are not true dangling bonds since this reconstruction has a semiconducting character with a band gap around 2.0 eV. Both occupied and empty levels are thus well separated from the Fermi level and, therefore, are expected to be less reactive than conventional, "metallic" dangling bonds. The "ball model" of Fig. 11 shows the close agreement between a multiple of the graphite unit vector length along the $\langle 10\bar{1}0 \rangle$ azimuth (13×2.459 Å = 31.97 Å) and six times the distance between silicon adatoms on top of the Si compact plane ($6 \times \sqrt{3} \times 3.07$ Å = 31.9 Å). The Si adatoms at the four edges of the represented graphene sheet coincide with troughs of the honeycomb graphite and are thus four nodes of the $(6\sqrt{3} \times 6\sqrt{3})R30°$ coincidence lattice. Although overlayer/substrate interactions are sufficiently weak to allow its unconstrained growth, the epitaxial layer is azimuthally oriented with respect to the substrate. A significant energy minimum configuration is thus obtained for the overlayer in the reported orientation which allows near commensurabil-

ity, the substrate acting as a template for the oriented growth. It is interesting to note that for the carbon-terminated $6H$-SiC $(000\bar{1})$ where the $\sqrt{3}$ reconstruction is not observed, the observation of ringlike structures in the diffraction pattern has been reported.[24] This confirms that the presence of the adatoms of the $\sqrt{3}$ reconstruction is essential to drive a preferred orientation during the growth of the first graphene sheet.

Nevertheless, a flagrant contradiction with the above-mentioned SXPS results remains to be clarified. These results suggest that graphitization is only revealed by heating to temperatures largely higher than 1150 °C, which is, however, sufficient for observing a well-developed $(6\sqrt{3} \times 6\sqrt{3})R30°$ diffraction pattern. How can we understand the seemingly delayed appearance of graphitization obtained by SXPS? We will begin by drawing a parallel evolution of our KRIPES spectra with the SXPS study of Johansson et al.[15] in this range of temperatures. Both studies reveal as early as 1080 °C the emergence of features that can be assigned to sp^2-hybridized carbon (peaks C and E on KRIPES spectra and component at 284.7 eV on the SXPS spectra) together with the development of other features which vanish at higher temperatures. This is the case of peak D and of the SXPS component located at 285.5 eV. Both structures first appear as a shoulder on the $\sqrt{3}$ spectra. Upon annealing in the range 1080–1150 °C, their intensity strongly increases, and peak D becomes dominant on KRIPES spectra in this domain of temperatures. At the same time, other features related to graphite progressively develop. Above 1250 °C, the intensity of D and of the peak at 285.5 eV on the SXPS spectra begins to decrease down to their almost complete disappearance at 1350 °C. At this stage we can observe fully developed graphite features on our KRIPES spectra while the SXPS spectra are dominated by a peak at 284.7 eV related to sp^2-hybridized graphitic carbon. In view of this parallelism, we suggest the following interpretation. The early emergence of the π^* states (Fig. 10) unambiguously shows that a graphite overlayer starts to develop on some terraces as soon as 1080 °C. The delayed appearance of peak F (σ^* states) above 1150 °C (Fig. 8) is clearly related to the growth of graphite multilayers. We propose that peak D, already present as a shoulder on the $(6\sqrt{3} \times 6\sqrt{3})R30°$ reconstruction but dominant in the range (1100,1250) °C, is characteristic of a strongly nonstoichiometric intermediate phase under the graphite overlayer. Indeed, its intensity progressively vanishes when the chemically modified substrate becomes buried under a graphite overlayer of growing thickness, becoming progressively out of reach of the low-energy electrons used in KRIPES.

We can now address more precisely the nature of the chemically perturbed subsurface region of the SiC substrate. We have seen that heat treatments at temperatures above 1000 °C induce Si evaporation and that this sublimation involves several layers of SiC in the bulk.[24] The rate of evaporation of Si from SiC has been estimated[12] using the vapor pressure data[44] of Drowart et al. For an annealing of 1030 °C, the evaporation rate of Si is 2.7×10^{12} atom cm^{-2} s^{-1}. This means that an annealing of 5 min at this temperature results in a calculated loss of Si of 2.7 monolayers. We can suppose that the first Si atoms to leave are the surface Si atoms and that a mechanism of Si

atom diffusion can be established under the surface up to the topmost layers where the Si atoms sublime. The large concentration of Si vacancies under the graphitic layer(s) can provide an explanation for the C $1s$ surface-shifted component at 285.5 eV recorded by SXPS on a surface presenting a fully developed $(6\sqrt{3} \times 6\sqrt{3})R30°$ LEED pattern. Indeed, in perfect SiC bulk, C atoms being more electronegative than Si atoms, there is a displacement of the electronic cloud from Si to C atoms.[45] In the presence of a Si vacancy, charge transfer can no longer occur so that C atoms ''lose'' some valence charge and C $1s$ shifts to larger binding energies. This charge relaxation near a Si vacancy can explain the presence of the component at 285.5 eV on the SXPS spectra. Furthermore, the quite large width of this component can be due to heterogeneous surroundings of the C atoms that could be surrounded by one, two, or three Si vacancies. The marked background detected on the $6\sqrt{3}$ LEED patterns is another signature of the incipient degree of disorder within this intermediate phase. In the limit of highly Si-defective layers, one may also envision the formation of a kind of diamond-like carbon phase made of several C-rich SiC bilayers with most of their C atoms sp^3-hybridized. This carbon-rich phase could then act as a precursor for the subsequent formation of a thermodynamically more stable graphite layer. An XPS study by Jackson et al.[46] on amorphous carbon thin films has shown that the C $1s$ spectrum is a superposition of three peaks which are assignable to sp^2-hybridized carbon (binding energy of 284.84 eV), sp^3-hybridized carbon at 285.80 eV, and an sp^2-satellite peak at 286.85 eV. The sp^3-hybridized carbon peak is thus shifted by ≈ 1 eV from the sp^2 peak towards increasing binding energy. This is fully compatible with the observation of the 285.5 eV component in the work of Johansson.

Within this Si vacancy model, the origin of peak D in the KRIPES spectra remains to be discussed. Electronic properties of native defects in cubic SiC have been calculated by Li et al.[47] Although their calculations were made for β-SiC, the essential features of the total density of states (see, e.g., Fig. 8 of Ref. 31) are expected to be roughly similar apart from the sensitive band-gap energy. They have determined the local density of states (LDOS) associated with each orbital at a given atomic site and also the changes (Δ-LDOS) associated with C or Si vacancy. At the neighboring of a Si vacancy, the Δ-LDOS essentially presents two peaks separated by 5.5 eV and located at ≈ 2 and 7.5 eV above the maximum of the valence band (E_{VBM}). We cannot directly compare this calculated LDOS with the density of states we have recorded at normal incidence in our KRIPES experiments because the reference energy is different in the two cases (E_F in our KRIPES study and E_{VBM} in the theoretical study). However, we can relate the two above-mentioned peaks of the Δ-LDOS with two peaks on our KRIPES spectra also separated by ≈ 5.5 eV. Peaks A and D at, respectively, 1 and 6.5 eV above E_F nicely satisfy this criterion. Figure 12 shows that peak A intensity closely follows that of peak D. Due to the presence of the surface-state peak U, structure A could not be detected before 1080 °C. Peak A clearly appears in the 1150 °C spectrum (Fig. 8) and undergoes a regular decrease in intensity down to its complete disappearance at 1350 °C. In Fig. 4 presenting spectra recorded on a graphitic surface annealed at 1400 °C, peak A was not needed to correctly fit
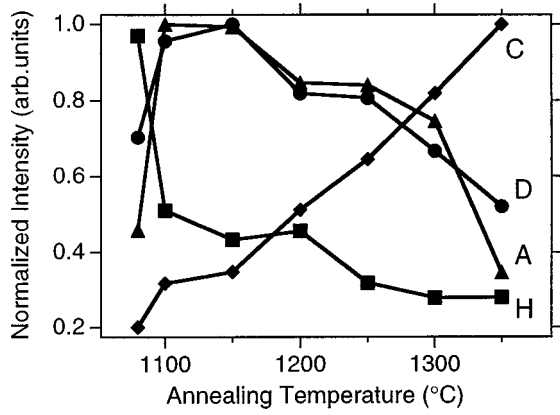
FIG. 12. Relative intensity variations of the main features (peaks *A*, *C*, *D*, and *H*) of the KRIPES spectra corresponding to Fig. 8 versus annealing temperature.

the spectra. It is thus obvious that this peak cannot be related to graphite. Instead, like peak *D*, it has to be related to the SiC substrate and to its associated changes in the density of states due to the presence of Si vacancies. In addition, the vanishing $k_\parallel$ dispersion of both peak *D* and *A* indicates that they both originate from electronic states with a localized or nonextended character. Let us point out that characteristic defect states in the conduction band have seldom been unambiguously attributed in the literature. Our observation opens the way for an improved comparison with more refined theoretical predictions of characteristic defect electronic properties and also to the quantitative evaluation of defect density.

Li *et al.*[47] have also calculated LDOS of *s* and *p* orbitals at Si and C sites and an average total electronic density of states of the cubic β-SiC polytype. The DOS of β-SiC presents a broad feature located at ≈ 8.5 eV above E_{VBM} mainly derived from *p* orbitals of C atoms. This state is shifted by ≈ 1 eV from the maximum in Δ-LDOS due to the presence of Si vacancies located at 7.5 eV we have just discussed. In Fig. 9, we can note that peak *H* is shifted by ≈ 1 eV away from peak *D* which we have assigned to Si vacancies. Peak *H*, already present in the $\sqrt{3}$ spectra and whose intensity decreases drastically with annealing upon 1080 °C, can only be related to SiC. Referring to the DOS calculated by Li *et al.*, and because of its position relative to peak *D*, feature *H* on KRIPES spectra can be ascribed to states which mainly derive from 2*p* orbitals of C atoms in SiC. The fast decrease of structure *H* visible in Fig. 9 confirms this origin. The interpretation of peak *H* as an intrinsic feature of SiC is also confirmed by recent band-structure calculations[48] of β-SiC, where three bands are located near 7.4 and 8.4 eV above E_{VBM}. In the vicinity of $\bar{\Gamma}$, their flat dispersion in the bulk BZ ΓL direction (perpendicular to the surface) gives rise to a high projected DOS which should ease their detection by KRIPES.

From all these observations, both peak *D* on KRIPES spectra and the broad surface component near 285.5 eV in the SXPS spectra must reflect the increasing number of Si vacancies in the C-rich SiC bilayers under the terminating graphitic layer(s) in formation. The observation of the feature *D* as a shoulder on the KRIPES $\sqrt{3}$ spectra means that there are already modified C-rich layers for this surface. However, we do not observe whatsoever any fingerprints of

graphite and the LEED pattern obtained for this reconstruction corresponds to the lattice parameters of SiC(0001). Therefore, the Si adatoms responsible for the formation of the $(\sqrt{3} \times \sqrt{3})R30°$ reconstruction are already supported by chemically perturbed layers with an already significant degree of nonstoichiometry. In the SXPS experiments also, the large broad feature which emerges near 285 eV was again already present on the $\sqrt{3}$ spectra. This is consistent with other AES results[9] which have suggested the presence of silicon vacancies in the terminating layer. In light of the present experiment, it is clear that these Si vacancies are to be found below the terminating layer of Si adatoms, which appears rather homogeneous as seen by STM.[20] Van Bommel has proposed a model for the graphitization of the 3*C*-SiC(111) surface: after sublimation of silicon, by annealing at 1200 °C, three successive carbon layers (total density$=3.67 \times 10^{15}$ atom cm^{-2}) collapse into a single layer of carbon (graphite type). This thesis is based on the very close value of the surface density of this single layer of carbon with the one of a graphite monolayer (3.80 $\times 10^{15}$ atom cm^{-2}). With the increase of annealing temperatures, the concentration of Si vacancy in the topmost layers increases so that there is a larger number of C atoms surrounded by Si vacancies. In the limit of high Si-vacancy concentration, the existence of an intermediate diamondlike-carbon phase is reflected in the growth of peak *D* in the KRIPES spectra, the presence of the component at 285.5 eV in the SXPS spectra, and the incoherent LEED background. Recent STM measurements[49] have also directly revealed a disordered phase when annealing a 4*H*-SiC(0001) face presenting a$(\sqrt{3} \times \sqrt{3})R30°$ reconstruction. With a further temperature increase, these highly defective layers collapse into a thermally stable single layer of graphite. Under this graphitic cover, with the increase of temperature, the mechanism of Si evaporation continues. Under the capping graphitic layer, there is still "formation" of C-rich layers which, in turn, can furnish additional graphite layers below the top monolayer, leading to the observed multilayer growth.

V. CONCLUSIONS

In summary, $k_\parallel$-resolved inverse photoemission spectroscopy applied to the $(6\sqrt{3} \times 6\sqrt{3})R30°$-reconstructed 6*H*-SiC(0001) surface has revealed a system of heteroepitaxial graphite overlayers above C-rich layers of a limited thickness. We are able to identify empty π^* states which are clear fingerprints of graphitic carbon for annealing temperatures as low as 1080 °C. The lack of significant energy shifts of these fingerprints reveals a weak interaction between the substrate and the overlayer, which has an electronic structure close to the "bulk" crystalline graphite. This weak interaction, which at first seems surprising for a compact terminating plane with a lot of dangling bonds, suggests that the growth of the first graphene sheet may proceed on top of adatoms characteristic of the $(\sqrt{3} \times \sqrt{3})R30°$ reconstruction which reduce the chemical reactivity of the substrate. This layer-by-layer growth opens up the possibility to isolate a single graphene sheet "floating" above the substrate. Further STM work is currently in progress to understand more fully these mechanisms. This kind of van der Waals epitaxial

process goes on upon annealing at increasing temperatures by formation of other graphite layers below the top graphene sheet. The results we have obtained for a low coverage of graphitic carbon reveal empty electronic states which can be related to structurally modified SiC bilayers under the graphitic layers. In particular, a critical role is played by silicon vacancies which show up as characteristic fingerprints in the KRIPES spectra. The SXPS spectra are readily understood considering a kind of diamondlike carbon phase which acts as a precursor to graphite formation. For higher annealing temperatures, KRIPES spectra are characteristic of multilayer graphite with a high degree of crystalline and azimuthal order.

Graphite has long been used in numerous adsorption studies as the archetype of a nonreactive substrate. However,

apart from sparse natural single crystals, it is usually found in the HOPG form with azimuthal misorientation within the layers. Since the details of the electronic structure, particularly in the empty states, are very sensitive to the structural quality of the surface, the present results also show that graphite thin films heteroepitaxially grown on silicon carbide are a substrate of choice for more refined adsorption studies which can now rely on an extended order over macroscopic dimensions.

*Author to whom correspondence should be addressed. Electronic address: themlin@gpec.univ-mrs.fr

[1] L. Edman, B. Sundqvist, E. McRae, and E. Litvin-Staszewska, Phys. Rev. B **57**, 6227 (1998).

[2] S. Saito, Science **278**, 77 (1997).

[3] M. S. Dresselhaus, G. Dresselhaus, and P. C. Eklund, *Science of Fullerenes and Carbon Nanotubes* (Academic, San Diego, 1996).

[4] J.-C. Charlier, X. Gonze, and J.-P. Michenaud, Phys. Rev. B **43**, 4579 (1991).

[5] J.-C. Charlier, X. Gonze, and J.-P. Michenaud, Europhys. Lett. **28**, 403 (1994).

[6] R. Claessen, H. Carstensen, and M. Skibowski, Phys. Rev. B **38**, 12 582 (1988).

[7] I. R. Collins, P. T. Andrews, and A. R. Law, Phys. Rev. B **38**, 13 348 (1988).

[8] H. Nishimito *et al.*, Rev. Sci. Instrum. **64**, 2857 (1993).

[9] V. M. Bermudez, Appl. Surf. Sci. **84**, 45 (1995).

[10] R. Kaplan and T. M. Parill, Surf. Sci. **165**, L45 (1986).

[11] U. Starke, C. Bram, P.-R. Steiner, W. Hartner, L. Hammer, K. Heinz, and K. Müller, Appl. Surf. Sci. **89**, 175 (1995).

[12] L. Muehlhoff, W. J. Choyke, M. J. Bozack, and J. T. Yates, J. Appl. Phys. **60**, 2842 (1986).

[13] R. Kaplan, Surf. Sci. **215**, 111 (1989).

[14] V. van Elsbergen, H. Nienhaus, and W. Mönch, Appl. Surf. Sci. **123/124**, 38 (1998).

[15] L. I. Johansson, F. Owman, and P. Mårtensson, Phys. Rev. B **53**, 13 793 (1996).

[16] L. I. Johansson, F. Owman, P. Mårtensson, C. Persson, and U. Lindefelt, Phys. Rev. B **53**, 13 803 (1996).

[17] L. Li and I. S. T. Tsong, Surf. Sci. **351**, 141 (1996).

[18] C. S. Chang, I. S. T. Tsong, Y. C. Wang, and R. F. Davis, Surf. Sci. **256**, 354 (1991).

[19] M.-H. Tsai, C. S. Chang, J. D. Dow, and I. S. T. Tong, Phys. Rev. B **45**, 1327 (1992).

[20] F. Owman and P. Mårtensson, Surf. Sci. **330**, L639 (1995).

[21] S. Tanaka, R. S. Kern, R. F. Davis, J. F. Wendelken, and J. Xu, Surf. Sci. **350**, 247 (1996).

[22] J. E. Northrup and J. Neugebauer, Phys. Rev. B **52**, R17 001 (1995).

[23] J.-M. Themlin, I. Forbeaux, V. Langlais, H. Belkhir, and J.-M. Debever, Europhys. Lett. **39**, 61 (1997).

[24] A. J. Van Bommel, J. E. Crombeen, and A. Van Tooren, Surf. Sci. **48**, 463 (1975).

[25] C. Klink, I. Stensgaard, F. Besenbacher, and E. Laegsgaard, Surf. Sci. **342**, 250 (1995).

[26] A. Nagashima, N. Tejima, Y. Gamou, T. Kawai, and C. Oshima, Phys. Rev. B **51**, 4606 (1995).

[27] K. Kobayashi and M. Tsukada, Phys. Rev. B **49**, 7660 (1994).

[28] H. Itoh, T. Ichinose, C. Oshima, T. Ichinokawa, and T. Aizawa, Surf. Sci. Lett. **254**, L437 (1991).

[29] A. Nagashima, K. Nuka, K. Satoh, H. Itoh, T. Ichinokawa, and C. Oshima, Surf. Sci. **287/288**, 609 (1993).

[30] S. Bouzidi, F. Coletti, J. M. Debever, P. A. Thiry, P. Dumas, and Y. J. Chabal, Phys. Rev. B **45**, 1187 (1992).

[31] C. H. Park, B.-H. Cheong, K.-H. Lee, and K. J. Chang, Phys. Rev. B **49**, 4485 (1994).

[32] M. A. van Hove, W. H. Weinberg, and C.-M. Chan, *Low-Energy Electron Diffraction* (Springer-Verlag, Berlin, 1992).

[33] F. Thibaudau (private communication).

[34] R. C. Tatar and S. Rabii, Phys. Rev. B **25**, 4126 (1982).

[35] N. A. W. Holzwarth, S. G. Louie, and S. Rabii, Phys. Rev. B **26**, 5382 (1982).

[36] T. Fauster, F. J. Himpsel, J. E. Fisher, and E. W. Plummer, Phys. Rev. Lett. **51**, 430 (1983).

[37] W. Eberhardt, I. T. McGovern, E. W. Plummer, and J. E. Fisher, Phys. Rev. Lett. **21**, 200 (1980).

[38] B. Reihl, J. K. Gimzewski, J. M. Nicholls, and E. Tosatti, Phys. Rev. B **33**, 5770 (1986).

[39] I. Schäfer, M. Schülter, and M. Skibowski, Phys. Rev. B **35**, 7663 (1987).

[40] D. Straub and F. J. Himpsel, Phys. Rev. B **33**, 2256 (1986).

[41] Y. Hu, T. J. Wagener, Y. Gao, H. M. Meyer III, and J. H. Weaver, Phys. Rev. B **38**, 3037 (1988).

[42] F. Maeda, T. Takahashi, H. Ohsawa, S. Suzuki, and H. Suematsu, Phys. Rev. B **37**, 4482 (1988).

[43] K. Ueno, M. Sakurai, and A. Koma, J. Cryst. Growth **150**, 1180 (1995).

[44] J. Drowart, G. deMaria, and M. G. Inghram, J. Chem. Phys. **29**, 1015 (1958).

[45] M. Sabisch, P. Krüger, and J. Pollmann, Phys. Rev. B **51**, 13 367 (1995).

[46] S. T. Jackson and R. G. Nuzzo, Appl. Surf. Sci. **90**, 195 (1995).

[47] Y. Li and P. J. Lin-Chung, Phys. Rev. B **36**, 1130 (1987).

[48] M. Rohlfing, P. Krüger, and J. E. Pollmann, Phys. Rev. B **48**, 17 791 (1993).

[49] T. Tsukamoto, M. Hirai, M. Kusaka, M. Iwami, T. Ozawa, T. Nagamura, and T. Nakata, Surf. Sci. **371**, 316 (1997).